# Asymptotic dynamics of higher-order lumps in the Davey–Stewartson II equation

IOP Publishing Journal of Physics A: Mathematical and Theoretical
J. Phys. A: Math. Theor. **55** (2022) 475701 (17pp) https://doi.org/10.1088/1751-8121/aca4a9

# Asymptotic dynamics of higher-order lumps in the Davey–Stewartson II equation

**Lijuan Guo[1], P G Kevrekidis[2] and Jingsong He[3,*]**

[1] College of Science, Nanjing Forestry University, Nanjing, Jiangsu 210037, People's Republic of China
[2] Department of Mathematics and Statistics, University of Massachusetts, Amherst, MA 01003-4515, United States of America
[3] Institute for Advanced Study, Shenzhen University, Shenzhen, Guangdong 518060, People's Republic of China

E-mail: hejingsong@szu.edu.cn and jshe@ustc.edu.cn

Received 30 May 2022; revised 26 October 2022
Accepted for publication 21 November 2022
Published 5 December 2022

**Abstract**

A family of higher-order rational lumps on non-zero constant background of Davey–Stewartson (DS) II equation are investigated. These solutions have multiple peaks whose heights and trajectories are approximately given by asymptotical analysis. It is found that the heights are time-dependent and for large time they approach the same constant height value of the first-order fundamental lump. The resulting trajectories are considered and it is found that the scattering angle can assume arbitrary values in the interval of $(\frac{\pi}{2}, \pi)$ which is markedly distinct from the necessary orthogonal scattering for the higher-order lumps on zero background. Additionally, it is illustrated that the higher-order lumps containing multi-peaked $n$-lumps can be regarded as a nonlinear superposition of $n$ first-order ones as $|t| \to \infty$.

Keywords: Davey–Stewartson II equation, Darboux transformation, lump, asymptotic analysis.

(Some figures may appear in colour only in the online journal)

* Author to whom any correspondence should be addressed.

## 1. Introduction

In this paper we consider the Davey–Stewartson (DS) II system, which was first derived by Davey and Stewartson to model water waves with weak surface tension [1]. This can also be considered as a long wave limit of Benney–Roskes equation [2] of the form:

$$\begin{aligned} &iu_t + u_{xx} - u_{yy} + (2\kappa|u|^2 + S)u = 0, \\ &S_{xx} + S_{yy} = -4\kappa(|u|^2)_{xx}, \quad \kappa = \pm 1, \end{aligned} \tag{1}$$

where $u$ is the amplitude of a surface wave packet and $S$ characterizes the mean motion generated by this surface wave. A recent discussion of the derivation of such models and their multiscale expansion connections can be found in the book of [3]. Apart from the realm of water waves, relevant models can be found to be relevant in other physical fields, such as nonlinear optics [4–6], plasma physics [7–9] and ferromagnets [10]. The system is integrable in that it admits Lax pair (see equations (6.1.2)–(6.1.3) in [11]) and can be solved via inverse spectral transformation with the help of the so-called $\bar{\partial}$ methods [12]. With regard to the solutions to DS II equation (1), the defocusing case ($\kappa = 1$) only admits line solitons, but does not possess lump solutions, as proved in [13]. Consequently, we limit our attention to the focusing case ($\kappa = -1$) to derive higher-order lumps and analyze their dynamics.

Lumps, as a class of rational soliton solutions, are localized in the all space and travel in time. An interesting topic in the realm of soliton dynamics (especially, in connection to such higher-dimensional settings) is to look at the scattering properties of two or more lump solitons colliding. The simplest type of interaction lumps was first discovered by Manakov *et al* in the Kadomtsev–Petviashvili (KP) equation by employing the dressing method [14]. Subsequently Satsuma and Ablowitz [15] used direct and long-wave limit methods to construct classes of lumps of the KP and DS equations. These solutions feature a trivial interaction, i.e. they consist of $n$ lumps traveling with distinct asymptotic velocities and their trajectories remain unchanged before and after interaction (i.e. for large time). In other words, they experience a normal scattering [16] and correspond to $n$-simple pole cases. Such interaction lump solutions on zero-boundary background of DS II were also obtained by Arkadiev *et al* via the inverse scattering method [17]. However, if the individual lumps have the same asymptotic center-of-mass velocities, they undergo anomalous scattering (an infinite phase shift of their trajectories) with a non-zero deflection angle after a head-on collision. These correspond to higher-order poles [18–20].

Many authors have also used different methods to study higher-order lumps of KP-I previously [16, 21, 22–29]. Gorshkov *et al* [16] reported a second-order lump solution which describes the nontrivial interaction and anomalous scattering of two lumps, which defied the paradigm of solitons as non-interacting entities. Ablowitz *et al* [20] used the inverse scattering transformation and binary Darboux Transformation to construct higher-order lumps that include the solution of [16] as a special case. They found that when $t$ runs from $-\infty$ to 0, these $n$ lump peaks first attract each other and overlap, after which time they experience a large angle scattering, then again separate into $n$ peaks as $t \to +\infty$. Other integrable equations such as the Boussinesq equation [30, 31], the $2+1$-dimensional NLS equation [32, 33], $2+1$-dimensional asymmetric Nizhnik–Novikov–Veselov system [34] and the $2+1$-dimensional chiral equation [35, 36] have also been found to feature similar solution structures. In [24, 27–29], the authors further found that the higher-order lumps split into a certain number of fundamental ones whose relative spatial separation grows in proportion to $|t|^q$ where $\frac{1}{3} \leqslant q \leqslant \frac{1}{2}$ as $|t| \to \infty$.

However, up to now, the asymptotic dynamics and scattering phenomena of the higher-order lumps of DS II equation were studied, to our knowledge, on a vanishing background. Mañas and Santini studied a large class of higher-order lumps on the zero background of the DS II equation with the use of a Wronskian scheme [37] and later different groups [38, 39] also used the inverse scattering method to construct such rational solutions. They behave highly nontrivially upon interaction (a head-on collision results in a orthogonal scattering). A natural question arises whether there exist novel lumps of DS II equation which feature anomalous scattering phenomena and scatter with non-orthogonal angle after collision. To this end, we need to construct a family of new rational lump solutions of DS II on a non-zero background and to explore their interactions which is a focal point of the present work.

The Darboux transformation (DT) has been used successively to obtain soliton, breather and rogue wave solutions in the last several years [40–52]. Given its earlier success, we utilize this method herein to construct higher-order rational lump solutions on non-zero constant background for DS II equation. To realize this goal, first we need to solve the Lax pair equations to find a hierarchy of solutions, which are used to construct more general DT. Indeed, one of our key results consists of the confirmation of the feature that arbitrary order Taylor coefficients of the fundamental eigenfunction (the usual exponential solution to Lax pair) all satisfy Lax pair equations with the same plane wave seeding solution.

Motivated by the above results, we shall concentrate on the following results.

- Beginning with the plane wave seeding solution, a hierarchy of new eigenfunctions generated by these Taylor coefficients of a usual exponential solution to the Lax pair, which are used to generalize the $n$-fold DT.
- Apart from the $\frac{\pi}{2}$ scattering occurring in collision between lumps [37, 38], we find a family of higher-order lumps on nonzero background of the DS II equation where the scattering angle can be an arbitrary constant in the interval of $(\frac{\pi}{2},\pi)$. The anomalous scattering and the time evolution process are illustrated by analyzing the approximate asymptotic formula of these lumps' trajectories.
- The approximate heights of these lump peaks evolve in time and approach the maximum value of the first-order fundamental lump as $|t|\to\infty$, which demonstrates how the $n$th-order lumps constitute a superposition of $n$ distinct peaks.

The rest of this paper is organized as follows. In section 2, we begin with the plane wave seeding solution, and establish that the Taylor coefficients of the fundamental eigenfunction all satisfy Lax pair equations. In section 3, the rational lump solutions up to the third-order are obtained by using DT, and their dynamical properties are studied. Our conclusions, as well as some potential directions of future study are given in the final section.

## 2. Eigenfunctions and Darboux transformation

The DS II equation (1) admits the following Lax pair equations [11]

$$\Psi_y = J\Psi_x + U\Psi, \quad \Psi_t = 2J\Psi_{xx} + 2U\Psi_x + V\Psi, \tag{2}$$

with a constant diagonal matrix $J=\begin{pmatrix} \mathrm{i} & 0 \\ 0 & -\mathrm{i} \end{pmatrix}$, and two potential matrices

$$U=\begin{pmatrix} 0 & u \\ v & 0 \end{pmatrix}, \quad V=\begin{pmatrix} (w+\mathrm{i}Q)/2 & u_x-\mathrm{i}u_y \\ v_x+\mathrm{i}v_y & (w-\mathrm{i}Q)/2 \end{pmatrix}. \tag{3}$$

Here, the vector $\Psi=(\psi,\phi)^T$ ($T$ denotes transpose), the potentials $u,\ v=-u^*\in\mathbb{C}$, and the field $Q=-2|u|^2+S\in\mathbb{R}$, are functions of the three independent variables $x,y,t$.

In this work, we restrict our attention to the plane wave seeding solution, i.e.

$$u=a\exp\left[\mathrm{i}(bx+cy+dt)\right],\quad v=-a\exp\left[-\mathrm{i}(bx+cy+dt)\right],\quad Q=b^2-c^2+d, \tag{4}$$

with $a,b,c,d\in\mathbb{R}$ and assume that the solution of the Lax pair is in the form of the following exponential function

$$\begin{aligned}\psi&=a_1\exp\left[\mathrm{i}(b_1x+c_1y+d_1t)\right],\\ \phi&=a_2\exp\left[\mathrm{i}(b_2x+c_2y+d_2t)\right],\end{aligned} \tag{5}$$

where $a_k\in\mathbb{R}$ and $b_k,c_k,d_k\in\mathbb{C}$ $(k=1,2)$. Insertion of this expression into the Lax pair (2), results in the parameters of the above fundamental eigenfunction $\Psi=(\psi,\phi)^T$ (column vector solution to Lax pair) satisfying:

$$\begin{aligned}&a_2=\frac{(b_1+\mathrm{i}c_1)a_1}{a},\quad c_1^{\pm}=\frac{c+\mathrm{i}b}{2}\pm\frac{\Xi}{2},\\ &d_1^{\pm}=b^2-2bb_1+\frac{d}{2}\pm\frac{(-\mathrm{i}b+c+2\mathrm{i}b_1)\Xi}{2},\\ &b_2=b_1-b,\quad c_2=c_1-c,\quad d_2=d_1-d,\\ &\Xi=\sqrt{4a^2+c^2-(b-2b_1)^2+2\mathrm{i}c(b-2b_1)}.\end{aligned}$$

For the sake of convenience, without loss of the generality of the possible dynamical behaviors for DS II equations, in what follows, we always select $b=c=d=0$, in which case the seeding solution becomes

$$u=-v=a,\quad Q=0, \tag{6}$$

and the exponential eigenfunction (5) reduces to

$$\begin{aligned}\psi^{\pm}&=\exp\left[\mathrm{i}b_1x\pm\sqrt{a^2-b_1^2}(\mathrm{i}y-2b_1t)\right],\\ \phi^{\pm}&=\frac{b_1\pm\sqrt{a^2-b_1^2}\mathrm{i}}{a}\exp\left[\mathrm{i}b_1x\pm\sqrt{a^2-b_1^2}(\mathrm{i}y-2b_1t)\right].\end{aligned} \tag{7}$$

By performing a Taylor expansion for the above exponential eigenfunction around the point $b_1=\lambda=\alpha+i\beta$ where $\alpha$ and $\beta$ are real constants and satisfy some constraints as seen in Remark 1, we have the power series:

$$\begin{aligned}\psi(b_1=\lambda+\epsilon)&=\psi^{[0]}+\psi^{[1]}\epsilon+\psi^{[2]}\epsilon^2+\cdots+\psi^{[N]}\epsilon^N+O(\epsilon^{N+1}),\\ \phi(b_1=\lambda+\epsilon)&=\phi^{[0]}+\phi^{[1]}\epsilon+\phi^{[2]}\epsilon^2+\cdots+\phi^{[N]}\epsilon^N+O(\epsilon^{N+1}),\end{aligned} \tag{8}$$

where $\psi^{[k]}=\frac{1}{k!}\frac{\partial^k\psi}{\partial b_1^k}|_{b_1=\lambda},\phi^{[k]}=\frac{1}{k!}\frac{\partial^k\phi}{\partial b_1^k}|_{b_1=\lambda},k=0,1,2,\cdots,N$ and $\varepsilon>0$ is an infinitesimal constant.

**Remark 1.** To obtain higher-order lumps of the DS II equation, the parameters $\alpha$ and $\beta$ satisfy that $\alpha$ is arbitrary when $\beta\neq0$, or $\alpha>a$ when $\beta=0$. In our paper, we focus on the case $\alpha=0,\beta\neq0$ below.

**Remark 2.** In what follows, since the derivation of the eigenfunction components $\psi$ and $\phi$ with respect to the parameter variable $b_1$ results in the singularity of the denominator (the denominator shall contain $\sqrt{a^2-b_1^2}$), we avoid the degenerate case scenario by assuming hereafter that $\alpha=0,\beta\neq0$ .

**Remark 3.** Assume that $(\psi,\phi)^T$ solves the Lax pair (2) with the seeding solution $u=-v=a, Q=0$. By performing a Taylor expansion as in equation (8), the arbitrary order Taylor coefficients $(\psi^{[k]},\phi^{[k]})^T$ are solutions to Lax pair with $u=-v=a, Q=0$. Based on the special seeding solution $u=-v=a$ (irrespectively of the expansion point $b_1\neq a$ as interpreted in remark 1) and the analyticity of the eigenfunction $\Psi$ (see equation (7)), one can conclude that all derivatives of $\Psi$ with respect to variable $b_1$ satisfy the linear Lax pair equation (2) with $u=-v=a$. Its Taylor coefficients $\Psi^{[k]}=(\psi^{[k]},\phi^{[k]})^T$ as above equation (8) are also solutions to the Lax pair equation (2) with the same seeding solution $u=-v=a$.

**Remark 4.** We just consider the case of $(\psi^+,\phi^+)^T$, and for simplicity, we still use $(\psi,\phi)^T$ instead of $(\psi^+,\phi^+)^T$ below. For the case with $(\psi^-,\phi^-)^T$ superscripts, the same dynamics of the solutions are obtained.

Remark 3 implies that there exists a hierarchy of eigenfunctions composed of Taylor coefficients for the same seeding solution. Based on the conclusion, the *n*th-order rational solution of the DS II equation generated by the *n*-fold DT (equation (49) in [40].) is generalized in the following Theorem.

**Theorem 1.** *Given the seeding solution $u=-v=a$ and choosing n distinct Taylor coefficients $\Psi^{[k_j]}=(\psi^{[k_j]},\phi^{[k_j]})^T$ $(k_j=1,2,\cdots,n)$ as eigenfunctions, then the new nth-order rational solution of DS II equation (1) is given by*

$$u^{[n]}=a+2\mathrm{i}\frac{\delta_2}{\delta_1} \tag{9}$$

*where*

$$\delta_1=\begin{vmatrix}
\partial_x^{n-1}\psi_1^{[k_1]} & \cdots & \partial_x^{n-1}\psi_n^{[k_n]} & \partial_x^{n-1}\phi_1^{[k_1]*} & \cdots & \partial_x^{n-1}\phi_n^{[k_n]*}\\
\partial_x^{n-2}\psi_1^{[k_1]} & \cdots & \partial_x^{n-2}\psi_n^{[k_n]} & \partial_x^{n-2}\phi_1^{[k_1]*} & \cdots & \partial_x^{n-2}\phi_n^{[k_n]*}\\
\vdots & \vdots & \vdots & \vdots & \vdots & \vdots\\
\psi_1^{[k_1]} & \cdots & \psi_n^{[k_n]} & \phi_1^{[k_1]*} & \cdots & \phi_n^{[k_n]*}\\
\partial_x^{n-1}\phi_1^{[k_1]} & \cdots & \partial_x^{n-1}\phi_n^{[k_n]} & -\partial_x^{n-1}\psi_1^{[k_1]*} & \cdots & -\partial_x^{n-1}\psi_n^{[k_n]*}\\
\partial_x^{n-2}\phi_1^{[k_1]} & \cdots & \partial_x^{n-2}\phi_n^{[k_n]} & -\partial_x^{n-2}\psi_1^{[k_1]*} & \cdots & -\partial_x^{n-2}\psi_n^{[k_n]*}\\
\vdots & \vdots & \vdots & \vdots & \vdots & \vdots\\
\phi_1^{[k_1]} & \cdots & \phi_n^{[k_n]} & -\psi_1^{[k_1]*} & \cdots & -\psi_n^{[k_n]*}
\end{vmatrix}$$

*and $\delta_2$ is the $n+1$ row of $\delta_1$ replaced by a row vector $\eta=(\partial_x^n\psi_1^{[k_1]},\cdots,\partial_x^n\psi_n^{[k_n]},\partial_x^n\phi_1^{[k_1]*},\cdots\partial_x^n\phi_n^{[k_n]*})$.*

**Remark 5.** Comparing with the *n*-fold DT (see equation (49) in [40].), we use here the Taylor coefficients as new eigenfunctions in order to construct a variety of solutions of DS II.

## 3. The higher-order lump solutions

For the DS II equations, under certain parameter restrictions, multi-lump solutions have been obtained in [15] on nonzero background. Later, Mañas and Santini employed a Wronskian scheme and Villarroel and Ablowitz employed the inverse scattering transformation and

Laurent coefficients to study the lump solutions on top of a zero background [37, 38]. They have found that some lumps described a non-trivial interaction, in other words, after a front collision, these lumps underwent scattering with a $\frac{\pi}{2}$ scattering angle. In the current work, we shall investigate higher-order lumps of the DS II equation on top of a nonzero constant background and show that they possess novel scattering where the scattering angle can be in the interval of $(\frac{\pi}{2},\pi)$.

### *3.1. The first-order fundamental lump*

In this part, without loss of diversity of dynamical behaviors of lump solutions, for simplicity, we choose the pure imaginary expanding point $\lambda = \mathrm{i}\beta$ in equation (8), i.e. $\alpha = 0$, and consider the following new moving coordinate frame

$$X = x, \quad Y = y - (4\beta + \frac{2a^2}{\beta})t. \tag{10}$$

The two eigenfunction components are given by the first-order Taylor coefficients

$$\begin{aligned} \psi_1 = \psi^{[1]} &= \frac{(\mathrm{i}MX + \beta Y)e^{\frac{\mathrm{i}(\mathrm{i}\beta^2 X + 2M^3 t + \beta MY)}{\beta}}}{M}, \\ \phi_1 = \phi^{[1]} &= \frac{(M+\beta)(1 - MX + \mathrm{i}\beta Y)e^{\frac{\mathrm{i}(\mathrm{i}\beta^2 X + 2M^3 t + \beta MY)}{\beta}}}{Ma}, \end{aligned} \tag{11}$$

with $M = \sqrt{a^2 + \beta^2}$. Then, insertion of $(\psi_1, \phi_1)^T = (\psi^{[1]}, \phi^{[1]})$ into the one-fold DT, equation (9) with parameters $n = 1, k_1 = 1$ yields a first-order fundamental lump solution

$$u^{[1]} = a\left[1 + \frac{-1 + 2\mathrm{i}\beta Y}{\left(MX - \frac{M+\beta}{2M}\right)^2 + \frac{a^2}{4M^2} + \beta^2 Y^2}\right]. \tag{12}$$

It was first obtained by Satsuma and Ablowitz by taking a 'long wave' limit of the corresponding one-soliton solution constructed by the direct method [15]. The solution is stationary in the moving coordinate $(X, Y)$-frame. It has a single maximum peak $\frac{(3M^2+\beta^2)}{a^2}|a|$ at $(\frac{M+\beta}{2M^2}, 0)$ and two local minima 0 at $(\frac{M+\beta}{2M^2} \pm \frac{\sqrt{3M^2+\beta^2}}{2M^2}, 0)$. Recalling the transformation connecting the moving frame to the rest one ($(x, y)$-plane), this first-order lump travels with a uniform velocity $(0, 4\beta + \frac{2a^2}{\beta})$. Its dynamics is illustrated in the $(X, Y)$-plane in figure 1.

**Remark 6.** In the above section, when $\lambda$ is real and $|\lambda| \leqslant |a|$, we observe that the line rogue wave solutions of DS II are obtained. On the other hand, we note that when $\lambda$ is a complex constant (or pure imaginary constant) and $|\lambda_{\Re}| > |a|$ (or $\lambda = \mathrm{i}\beta$) where $\lambda_{\Re}$ denotes the real part of $\lambda$, the lump solutions of DS II are derived, i.e. the character of the solutions changes depending on the specific selection of $\lambda$ within the complex plane.

**Remark 7.** In what follows, we shall set $a > 0$ and $\beta > 0$ without loss of generality.

### *3.2. The second-order non-fundamental lump*

This part is devoted to using one- and two-fold DT to construct two second-order non-fundamental lump solutions and study their dynamical properties. For the sake of convenience, the discussion is considered in the moving coordinate frame (10) below.

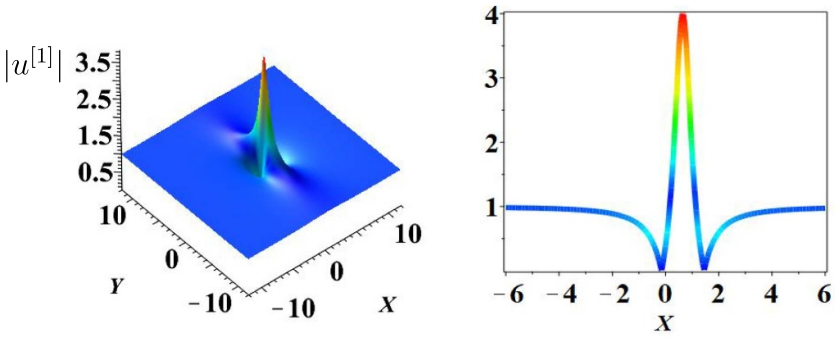


**Figure 1.** (a) The first-order lump of the DS II equation with parameters $a = 1, \beta = \frac{1}{2}, M = \frac{\sqrt{5}}{2}$, (b) the $Y$-crossection showing one maximum and two minima.

*3.2.1. Case 1 the second-order lump using one-fold DT.* In this case, choosing the following set of parameters in equation (9)

$$\lambda_1 = \mathrm{i}\beta(\beta > 0), \quad n = 1, \quad k_1 = 2, \tag{13}$$

then the one-fold DT yields a second-order non-fundamental lump solution. Because of the cumbersome expression of this solution, we just provide here the corresponding eigenfunctions

$$\begin{aligned}\psi^{[2]} =& \frac{\mathrm{i}(2M^2\beta^2XY - 2M^4t + 6M^2\beta^2t - M^2\beta Y + \beta^3Y + \mathrm{i}M^3\beta^2X^2 - \mathrm{i}M\beta^3Y^2)e^{-\beta^2X+\mathrm{i}(2M^3t+M\beta Y)}}{2M^3\beta},\\ \phi^{[2]} =& \frac{(M+\beta)\mathrm{i}}{a}\psi^{[2]} + \frac{\left[\mathrm{i}M^2X + (\beta Y - \frac{\mathrm{i}}{2})M + \frac{\mathrm{i}\beta}{2}\right](M+\beta)e^{-\beta^2X+\mathrm{i}(2M^3t+M\beta Y)}}{M^3\beta}.\end{aligned} \tag{14}$$

Distinctly from the first-order case, the two eigenfunction components are dependent on $t$, so the solution is non-stationary in the moving coordinate frame. When $|t| \to \infty$, it contains two separated individual lump peaks, while in the intermediate times, the two lump peaks fuse together. In order to analyze their interaction process, their heights and the traveling paths of the two local maxima for the two lump peaks need to be determined. Since the exact analytical formulas are very complicated to obtain, we make the following reductions. Taking into consideration the expression

$$u^{[2]} = a - 2\mathrm{i}\frac{\psi^{[2]}\phi_X^{[2]*} - \phi^{[2]}\psi_X^{[2]*}}{|\psi^{[2]}|^2 + |\phi^{[2]}|^2}, \tag{15}$$

the maximum of $|u^{[2]}|$ shall occur near the minimum of the denominator which is approximately at the zeros of the leading terms of this polynomial part.

Solving $|\psi^{[2]}| = 0$, when $\beta > 0, M^2 - 3\beta^2 = a^2 - 2\beta^2 > 0$, for large time $|t|$, we identify the two lump peaks whose maximum asymptotic coordinates are given by

$$X = \pm\frac{\sqrt{-M\beta(M^2-3\beta^2)t}}{M\beta} + \frac{a^2}{4\beta M^2} + \frac{M+\beta}{2M^2}, \quad Y = -\frac{M}{\beta}X + \frac{M+\beta}{2M\beta}, \quad t \to -\infty, \tag{16}$$

and

$$X = \pm\frac{\sqrt{M\beta(M^2-3\beta^2)t}}{M\beta} + \frac{a^2}{4\beta M^2} + \frac{M+\beta}{2M^2}, \quad Y = \frac{M}{\beta}X - \frac{M+\beta}{2M\beta}, \quad t \to +\infty, \tag{17}$$

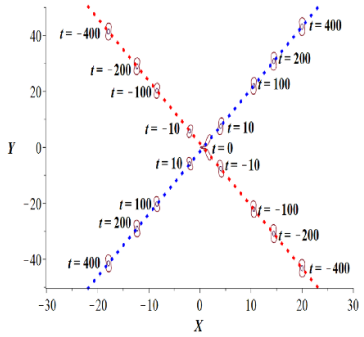


**Figure 2.** The time evolution of the second-order lump of equation (15). The contour plots of these lumps at distinct times is plotted using the exact analytical solution (15) by leveraging the eigenfunction of equation (14), and the two dot straight lines denote the two asymptotic lines given by equations (16) and (17).

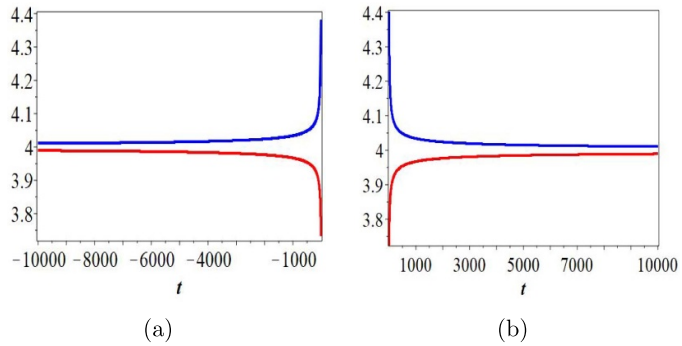


**Figure 3.** (a) the two maximum amplitude values of the two lumps from $t=-10000$ to $t=-10$, (b) the two maximum amplitude values of the two lumps from $t=10$ to $t=10000$.

with $M=\sqrt{a^2+\beta^2}$. It is confirmed by direct comparison with the numerical profiles of the exact solutions that these approximate asymptotic expressions adequately reflect the lump center positions for all times as shown in figure 2.

Before studying the maximum amplitudes of the two lumps, we take $a=1,\beta=\frac{1}{2},M=\frac{\sqrt{5}}{2}$. Substituting the asymptotic coordinates (16) and (17) into the solution $u^{[2]}$ (15), the amplitude of one lump is larger than 4 and approaches 4, whereas for the other one, the amplitude is less than 4 and approaches 4 as $t\to-\infty$. The same conclusion holds as $t\to+\infty$, as shown in figure 3. Notice there is a slight deviation of our above asymptotic expressions from the limiting value, given their approximate nature.

From equations (16) and (17), the asymptotic trajectories define two straight lines with different slopes for $t\to\pm\infty$. More concretely, the asymptotic line for $t\to+\infty$ is obtained from the line for $t\to-\infty$ by reflection with respect to the $X$-axis, and the angle between the two asymptotic lines is denoted by $\Theta$. Since the two lump peaks first experience a head-on collision henceforth undergoing a scattering process, according to the coordinates (16) and (17), the scattering angle $\Theta$ is given by

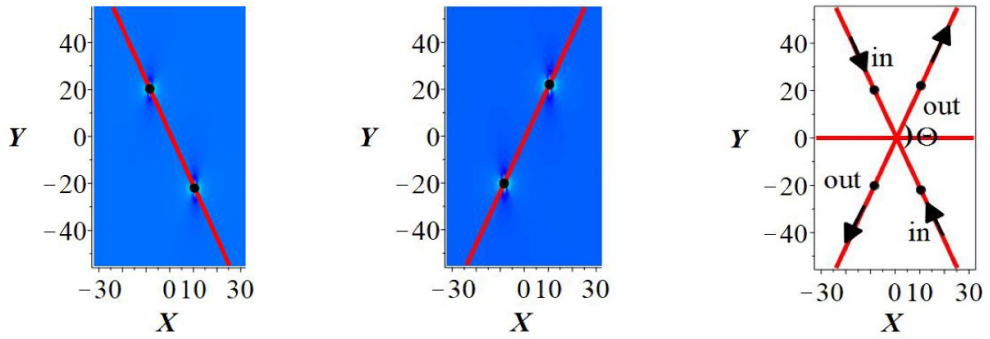


(a) (b) (c)

**Figure 4.** Location of the two pulses: (a) incoming ($t=-100$) and (b) outgoing ($t=100$) with parameters $a=1,\beta=\frac{1}{2},M=\frac{\sqrt{5}}{2}$. (c) The nontrivial collision process of before ($t\to-\infty$) and after ($t\to+\infty$) scattering and the angle is indicated, and when $|t|=100$, these two lumps nearly totally locate at the two straight lines. In panel (c), a schematic of the incoming and outgoing wave angles is provided.

$$\cos\Theta=-\frac{a^2}{a^2+2\beta^2}. \tag{18}$$

Here $\cos\Theta$ reaches to the minimum value $-1$ as $a\to\infty$ and attains a maximum value 0 as $a$ goes to 0; in other words, the scattering angle $\Theta\in(\frac{\pi}{2},\pi)$. Figure 4 shows the traveling paths of the two lump peaks before and after collision. It is seen that the two lumps located at the second and fourth quadrants first accelerate and approach each other along a straight line. After a front collision and undergoing a large scattering angle, they decelerate and move away each other along the other straight line (among the ones given above) and, finally, they move along the first and third quadrants. Also, the approximate estimations of the center positions are nearly coincident with the exact ones illustrated by the density plots.

Reverting back to the rest coordinate $(x,y)$-frame, from equation (10), the peak locations are given by $(x,y)=(X,\frac{2a^2t+4\beta^2t+\beta Y}{\beta})$ when $|t|\gg0$. The corresponding coordinate $y$ satisfies the following equations,

$$\begin{aligned}\beta y&=\left(2a^2+4\beta^2\right)t-Mx+\frac{M+\beta}{2M}, &&t\to-\infty,\\ \beta y&=\left(2a^2+4\beta^2\right)t+Mx-\frac{M+\beta}{2M}, &&t\to+\infty,\end{aligned} \tag{19}$$

where $t$ can given by solving equations (16) and (17), i.e.

$$|t|=\frac{\sqrt{M\beta}}{M^2-3\beta^2}\left[x-\frac{a^2+2\beta(M+\beta)}{4\beta M^2}\right]^2 \tag{20}$$

with $M>0,\beta>0$ and $M^2-3\beta^2>0$ when $a^2>2\beta^2$. Combining equations (19) and (20), it is found that the two lumps locate at two parabolas in the $(x,y)$-plane, which is illustrated in figure 5.

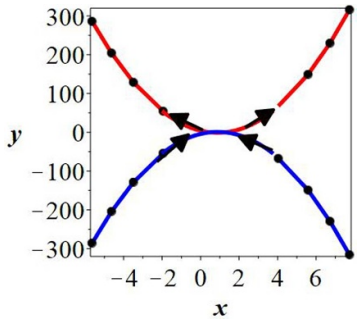


**Figure 5.** The second-order lump peak trajectories with parameters $a = 1, \beta = \frac{1}{2}$ and $M = \frac{\sqrt{5}}{2}$ in the $xy$-plane. The blue parabolic curve is given by the first formula of equations (19) and (20), the red parabolic curve is given by the second formula of equations (19) and (20), and the black points describe the peak coordinates.

*3.2.2. Case 2 the second-order lump using two-fold DT.* To compare with the second-order lump in Case 1, we choose the following set of parameters in equation (9)

$$\lambda_2 = \lambda_1 = \mathrm{i}\beta, \quad n = 2, \quad k_1 = 1, \quad k_2 = 2. \tag{21}$$

A new second-order lump is obtained by using the two-fold DT. For large time $t$, this solution features a generally opposite time evolution process in comparison to the Case 1 above, that is, when $t \to -\infty$ the two lump peaks locate at the first and third quadrants whereas they move to the second and fourth quadrants as $t \to +\infty$. To demonstrate this phenomenon, the asymptotical trajectories of these two lump peaks are determined. Similarly to our discussion above, the approximate coordinates of the maxima of two lumps are given by

$$X = \pm\frac{\sqrt{-M\beta(M-3\beta^2)t}}{M\beta} - \frac{a^2}{4M^2\beta} + \frac{M+\beta}{2M^2}, \quad Y = \frac{M}{\beta}X - \frac{M+\beta}{2M\beta}, \quad t \to -\infty, \tag{22}$$

and

$$X = \pm\frac{\sqrt{M\beta(M^2-3\beta^2)t}}{M\beta} - \frac{a^2}{4M^2\beta} + \frac{M+\beta}{2M^2}, \quad Y = -\frac{M}{\beta}X + \frac{M+\beta}{2M\beta}, \quad t \to +\infty. \tag{23}$$

where $M = \sqrt{a^2+\beta^2}$ and $\sqrt{M\beta(M^2-3\beta^2)|t|}$ is well-defined as $a^2 > 2\beta^2$. In this case, the scattering angle is given by

$$\cos\theta = -\frac{a^2}{a^2+2\beta^2}. \tag{24}$$

This asymptotic dynamics is illustrated in figure 6. It is clearly seen that these approximate estimations are in good agreement with the exact solution illustrated by the density plot. Furthermore, comparing figures 6(c) with 4(c), it is also found that the second-order lump obtained by using the one-fold DT evolves effectively in a time-reversed way in comparison with the one obtained by using two-fold DT (see also equations (16), (23) and equations (17), (22), respectively).

**Remark 8.** Though the two scattering angles in Case 1 and Case 2 are the same (see equations (18) and (24)), the directions of incoming and outgoing waves are opposite. Also,

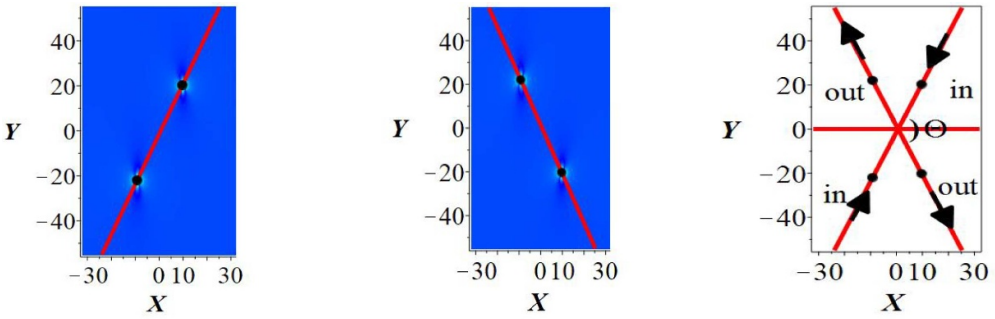


(a) (b) (c)

**Figure 6.** Location of the two pulses: (a) incoming ($t=-100$) and (b) outgoing ($t=100$) with parameters $a=1,\beta=\frac{1}{2},M=\frac{\sqrt{5}}{2}$. (c) The nontrivial collision process of before ($t=-\infty$) and after ($t=+\infty$) scattering and the angle is indicated. When $|t|=100$, these two lumps are practically located at two straight lines. The scattering angle is also indicted by $\Theta$.

the scattering angle is not necessarily normal, which is a central difference of the results herein from the one of two lumps for DS II equation on zero background [37, 38].

### 3.3. *The non-fundamental third-order lump*

The third-order lump and its asymptotics can be studied in the same manner as in the second-order lump case, and for this reason we omit here some of the technical details. To illustrate its dynamical evolution process and asymptotic heights, the locations of the three lump peaks shall be given.

*3.3.1. Case 3 the third-order lump using the one-fold DT.* With the choice of the following set of parameters in equation (9):

$$\lambda_1=\mathrm{i}\beta,\quad n=1,\quad k_1=3, \tag{25}$$

a third-order lump $u^{[3]}$ is obtained by using one-fold DT. The following eigenfunctions are used,

$$\psi^{[3]}=-\frac{1}{6M^5\beta}\left(\psi_{\mathrm{Re}}^{[3]}+\mathrm{i}\psi_{\mathrm{Im}}^{[3]}\right)e^{\xi},\quad \phi^{[3]}=\frac{-\mathrm{i}(M+\beta)}{M^5\beta a}\left(\phi_{\mathrm{Re}}^{[3]}+\mathrm{i}\phi_{\mathrm{Im}}^{[3]}\right)e^{\xi}, \tag{26}$$

with

$$\begin{aligned}
\xi&=-\beta^2X+\mathrm{i}(M\beta Y+2M^3t),\quad M=\sqrt{a^2+\beta^2},\\
\psi_{\mathrm{Re}}^{[3]}&=3\beta^2M^4X^2Y-\beta^4M^2Y^3-6M^6tX+18M^4\beta^2tX-3\beta M^4XY+3\beta^3M^2XY\\
&\quad-12\beta M^4t+12\beta^3M^2t-3\beta^2M^2Y+3\beta^4Y,\\
\psi_{\mathrm{Im}}^{[3]}&=M\beta(M^4X^3-3\beta^2M^2XY^2+6M^4tY-18\beta^2M^2tY+3M^2\beta Y^2-3\beta^3Y^2),\\
\phi_{\mathrm{Re}}^{[3]}&=\psi_{\mathrm{Re}}^{[3]}-6\beta^2M^3XY+6M^5t-18M^3\beta^2t+3\beta M^3Y+3\beta^2M^2Y-6\beta^3MY,\\
\phi_{\mathrm{Im}}^{[3]}&=\psi_{\mathrm{Im}}^{[3]}-3\beta M^4X^2+3M^2\beta^3Y^2+3M^3\beta X-3\beta^2M^2X+3M\beta^2-3\beta^3.
\end{aligned}$$

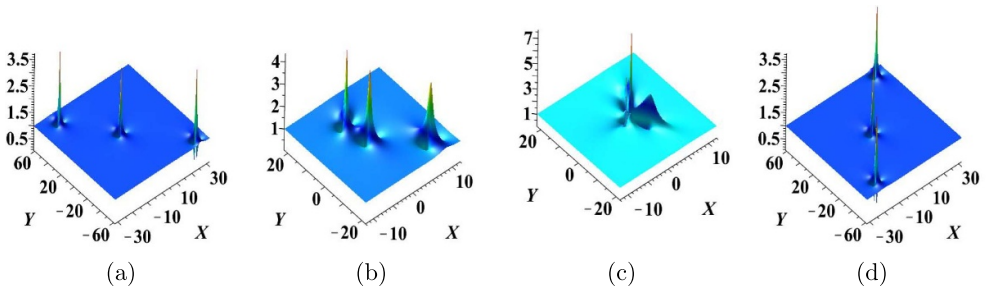


**Figure 7.** The time evolution process of the third-order lump obtained by using the one-fold DT with parameters $a=1, \beta=\frac{1}{2}$ and $M=\frac{\sqrt{5}}{2}$ at distinct time. (a) $t=-200$; (b) $t=-10$; (c) $t=0$; (d) $t=200$.

For large $t$, this solution is split into three lumps whose asymptotic coordinates of the maxima are given by

$$\begin{cases} X_{1,2}=\pm\dfrac{\sqrt{3M\beta(M^2-3\beta^2)t}}{M\beta}+\Delta+\dfrac{M-\beta}{3M\beta}, \quad Y=-\dfrac{M}{\beta}X_{1,2}+\dfrac{M+\beta}{M\beta}+\dfrac{a^2}{4M\beta}, \\ X_3=-\dfrac{M+\beta}{3M}, \quad Y_3=-\dfrac{M}{\beta}X_3-\dfrac{M+\beta}{2M\beta}-\dfrac{a^2}{3M\beta}, \end{cases} \quad t\to-\infty, \tag{27}$$

and

$$\begin{cases} X_{1,2}=\pm\dfrac{\sqrt{-3M\beta(M^2-3\beta^2)t}}{M\beta}+\Delta+\dfrac{M-\beta}{3M\beta}, \quad Y=\dfrac{M}{\beta}X_{1,2}-\dfrac{M+\beta}{M\beta}-\dfrac{a^2}{4M\beta}, \\ X_3=-\dfrac{M+\beta}{3M}, \quad Y_3=\dfrac{M}{\beta}X_3+\dfrac{M+\beta}{2M\beta}+\dfrac{a^2}{3M\beta}, \end{cases} \quad t\to+\infty, \tag{28}$$

where $\Delta=\frac{3(M+\beta)(M\beta+M-\beta)}{4M^2\beta}$ and when $a^2>2\beta^2$ the quantity $\sqrt{3M\beta(M^2-3\beta^2)|t|}$ is well defined. The dynamics of this third-order lump is illustrated in figure 7. Figure 8 shows that the exact (density figures) and approximate peak locations (red, blue and black points) are generally in good agreement for large $|t|$. When $t\ll 0$, the three lump peaks are separated and two of them are located at the second and fourth quadrants. Subsequently they approach and eventually overlap with the middle one. As time progresses, the three lump peaks again split into three distinguishable peaks, with the middle one remaining fixed while the other two peaks separate from each other and move to the first and third quadrants. Note that the two peaks (located at the first and third quadrants (or the second and fourth quadrants) move along two distinct straight lines but their slopes are same with the corresponding second-order lump obtained by using one-fold DT (see also equations (16), (17) and (27), (28)). Furthermore, the approximate heights of the three lump peaks are also calculated by substituting the asymptotic coordinates into the expression of the third-order lump solution, as illustrated in figure 9. It is seen that (a) each peak height approaches the asymptotic value 4 where the minor difference comes from the approximate coordinate estimate (similarly to what was discussed before) of lump peaks; (b) the peak height (red point) grows as time evolves whereas the other one (blue point) decreases as $t\ll 0$, but the peak height (red point) decreases as time evolves whereas the other one (blue point) grows for $t\gg 0$. Moreover, the middle one (black point) generally remains unchanged during the evolution process.

**Remark 9.** The trajectories of the three lump peaks in the $xy$-plane can be obtained using (10), (27) and (28) as in the two-lump case but are not shown here.

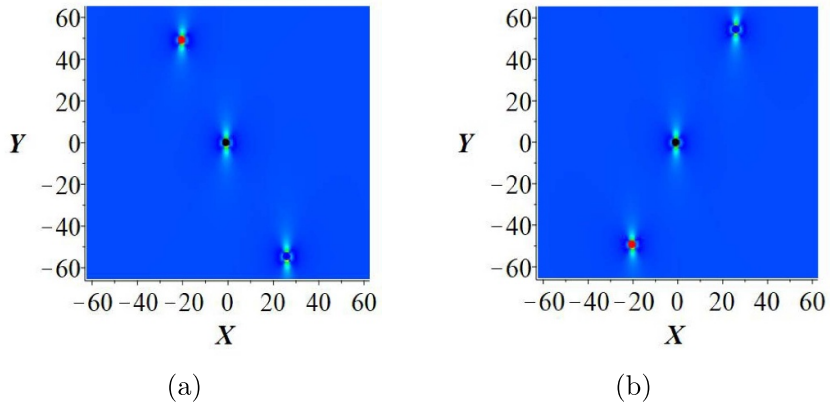


**Figure 8.** Location of the three lump peaks in Case 3: (a) $t=-200$, (b) $t=200$. The black point represents the location of the fixed lump; the red point denotes the approximate coordinates of one lump, and the blue point denotes the approximate coordinates of the other lump.

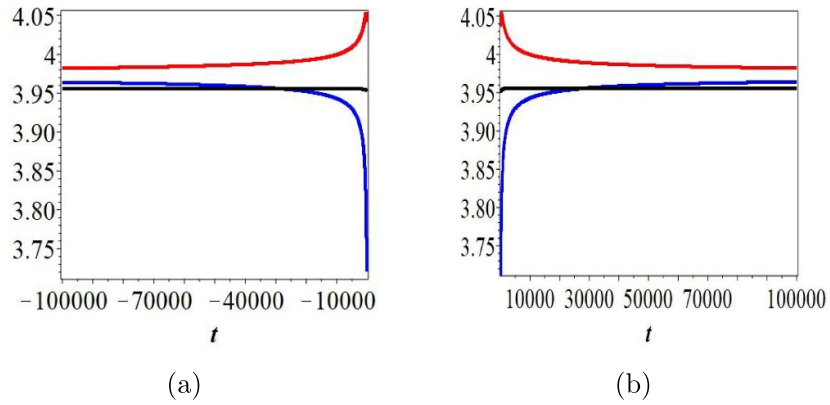


**Figure 9.** The evolution of the heights of the three lump peaks over time: (a) from $t=-100\,000$ to $t=-200$, (b) from $t=200$ to $t=100\,000$. The black line represents the height of the fixed lump; the red line denotes the height of second lump, and the blue line denotes the height of the third lump.

*3.3.2. Case 4 the third-order lump using three-fold DT.* Comparing with the third-order lump obtained by using the one-fold DT in Case 3, in the present case, we shall use the three-fold DT to construct a similar third-order lump, but which possesses a generally 'opposite' time evolution process. That is, when $t\ll 0$ two lumps are located at the first and third quadrants whereas they move to the second and fourth quadrants as $t\gg 0$, with the middle lump remaining still during the entire time evolution.

Choosing the following set of parameters in equation (9)

$$\lambda_1=\lambda_2=\lambda_3=\mathrm{i}\beta,\quad n=3,\quad k_1=1,\quad k_2=2,\quad k_3=3, \tag{29}$$

a third-order lump $\widetilde{u^{[3]}_{\mathrm{lump}}}$ of DS II is obtained by using three-fold DT. Since the expression of this solution is lengthy and complex, once again we leverage the analytical means of approximating the trajectories and heights of the three lump peaks similarly to previous cases. Indeed, we omit lengthy details but only

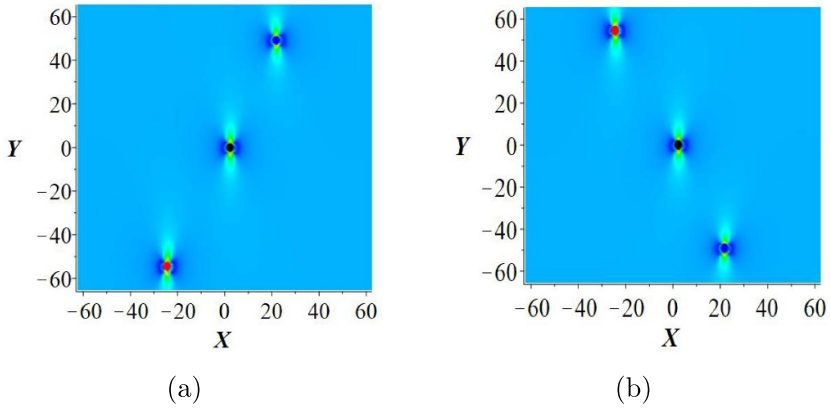


**Figure 10.** Location of the three lump peaks in Case 4: (a) $t=-200$, (b) $t=200$. The black point represents the location of the fixed lump; the red points denote the approximate coordinates of the second lump, and the blue points denote the approximate coordinates of the third lump.

focus on some relevant results for the time evolution of the lump peaks. For large $t$, the approximate coordinates of these three lumps are given by

$$\begin{cases} X_{1,2}=\pm\dfrac{\sqrt{-3M\beta(S^2-3\beta^2)t}}{M\beta}-\Delta+\dfrac{M-\beta}{M^2\beta}, \quad Y=\dfrac{M}{\beta}X_{1,2}+\dfrac{M+\beta}{M\beta}-\dfrac{3a^2}{2M\beta}, \\ X_3=\Delta, \quad y=\dfrac{M}{\beta}X_3-\dfrac{2(M+\beta)}{M^2\beta}, \end{cases} \quad t\to-\infty, \quad (30)$$

and

$$\begin{cases} X_{1,2}=\pm\dfrac{\sqrt{3M\beta(S^2-3\beta^2)t}}{M\beta}-\Delta+\dfrac{M-\beta}{M^2\beta}, \quad Y=-\dfrac{M}{\beta}X_{1,2}-\dfrac{M+\beta}{M\beta}+\dfrac{3a^2}{2M\beta}, \\ X_3=\Delta, \quad y=-\dfrac{M}{\beta}X_3+\dfrac{2(M+\beta)}{M^2\beta}, \end{cases} \quad t\to+\infty, \quad (31)$$

where $\Delta=\frac{3(M+\beta)(M\beta+M-\beta)}{4M^2\beta}$ and when $a^2>2\beta^2$ the quantity $\sqrt{3M\beta(M^2-3\beta^2)|t|}$ is well defined. When $|t|=200$ the exact analytical solution and approximate coordinates (30) and (31) are plotted in figure 10. It is seen that when $t<0$ the two lumps are located in the first and third quadrants whereas they move to the second and fourth quadrants after the collision, which is confirmed by figure 10. By a close observation, we find the evolutions of profile in figures 8 and 10 are opposite approximately along time $t$. For example, figure 8(a) for t$=-200$ is corresponding to figure 10(b) for $t=200$. But, comparing with equations (27) and (31), one can find that for the same $|t|$, these peak coordinates in the two cases are not totally uniform. In other words, the modulus of the third-order lump $u^{[3]}$ with parameters (25) is not equal to that one of the third-order lump $\widetilde{u^{[3]}}$ with parameters (29) at the same $|t|$ (i.e. $|u^{[3]}(x,y,t)|\neq|\widetilde{u^{[3]}}(x,y,-t)|$). The heights of three peaks can be computed by inserting the approximate coordinates into the expression of this solution, hence we do not repeat this step here.

**Remark 10.** These cases further demonstrate that the scattering process does not necessarily occur at normal angles for the multi-lump solutions of the DS II equation, a key finding of the present work.

## 4. Conclusion and discussion

In this paper, we showed the asymptotic properties of the newly obtained family of the higher-order lump solutions for the DS II equation in the moving coordinate frame (10). For the higher-order lump, when $|t| \to \infty$ we find that it splits into multi-peak lumps whose heights evolve with time and approach the same constant value corresponding to that of the simple first-order fundamental lump, and the peak trajectories have a time dependence that grows as $\sqrt{|t|}$, a feature similar to what has been found for the KP I equation [18–20] and for higher-order lumps on zero background of the DS II equation [38]. Nevertheless, they define straight lines with different slopes for $t \to \pm\infty$. The lumps are found to collide head-on undergoing a scattering process, and the scattering angle $\Theta \in (\frac{\pi}{2}, \pi)$ is identified herein as being different from the higher-order lump on the zero background case where the scattering must be orthogonal. Besides, though we just discussed solutions up to the third-order, $n$th-order lumps can be obtained by using the $n$-fold DT (9). Generalizing the results obtained herein to arbitrary $n$ would be an interesting topic for further study.

Our results concerning the dynamics for rational solutions of DS II can be a basis for corresponding observations in areas of application where the DS II is relevant, including most notably in nonlinear optics and plasma physics, among others. The method of construction and asymptotical analysis of exact solutions of the DS II in this paper can also be widely used to other $2+1$ dimensional integrable systems, such as the KP equation, the $2+1$ dimensional Fokas equation, etc. Indeed, this prompts theoretical, numerical and even experimental studies to consider the angle of interaction of lump-like solutions that can arise in settings that bear such solutions.

## Data availability statement

No new data were created or analyzed in this study.

## Acknowledgments

This work is supported by the National Natural Science Foundation of China (Grants 12071304 and 12101312). The Natural Science Foundation of Jiangsu Province of China (Grant BK20210606) and the Natural Science Foundation of the Jiangsu Higher Education Institutions of China (Grant 21KJB110030). This material is also based upon work supported by the US National Science Foundation under Grant No. DMS-2204702 (P G K ).

## ORCID iDs

P G Kevrekidis https://orcid.org/0000-0002-7714-3689
Jingsong He https://orcid.org/0000-0002-2068-1849

## References

[1] Davey A and Stewartson K 1974 On three-dimensional packets of surface waves *Proc. R. Soc.* A **338** 101–10
[2] Benney D J and Roskes G J 1969 Wave instability *Stud. Appl. Math.* **47** 377–85
[3] Ablowitz M J 2011 *Nonlinear Dispersive Waves: Asymptotic Analysis and Solitons* (Cambridge: Cambridge University Press) ch 6.8.
[4] Newell A C and Moloney J V 1992 *Nonlinear Optics* (Redwood City, CA: Addison-Wesley)
[5] Ablowitz M J, Biondini G and Blair S 2001 Nonlinear Schrödinger equation with mean terms in nonresonant multidimensional quadratic materials *Phys. Rev.* E **63** 046605

[6] Ablowitz M J, Bakirtas I and Ilan B 2007 On a class of nonlocal nonlinear Schrödinger equations and wave collapse *Eur. Phys. J.: Spec. Top.* **147** 343–62
[7] Zakharov V E, Musher S L and Rubenchik A M 1985 Hamiltonian approach to the description of non-linear plasma phenomena *Phys. Rep.* **129** 285–366
[8] Nishinari K, Abe K and Satsuma J 1993 A new-type of soliton behavior in a two dimensional plasma system *J. Phys. Soc. Japan* **62** 2021–9
[9] Panguetna C S, Tabi C B and Kofané T C 2017 Two-dimensional modulated ion-acoustic excitations in electronegative plasmas *Phys. Plasmas.* **24** 092114
[10] Leblond H 1999 Electromagnetic waves in ferromagnets *J. Phys. A: Math. Theor.* **32** 7907–32
[11] Matveev V B and Salle M A 1991 *Darboux Transformations and Solitons* (Berlin: Springer)
[12] Fokas A S and Ablowitz M J 1984 On the inverse scattering transform of multidimensional nonlinear equations related to first-order systems in the plane *J. Math. Phys.* **25** 2494–505
[13] Beals R and Coifman R R 1986 The D-bar approach to inverse scattering and nonlinear evolutions *Physica* D **18** 242–9
[14] Manakov S V, Zakharov V E, Bordag L A, Its A R, Matveev V B 1977 Two-dimensional solitons of the Kadomtsev–Petviashvili equation and their interaction *Phys. Lett.* A **63** 205–6
[15] Satsuma J and Ablowitz M J 1979 Two-dimensional lumps in nonlinear dispersive systems *J. Math. Phys.* **20** 1496–503
[16] Gorshkov K A, Pelinovsky D E and Stepanyants Yu A 1993 Normal and anomalous scattering, formation and decay of bound states of two-dimensional solitons described by the Kadomtsev–Petviashvili equation *J. Exp. Theor. Phys.* **77** 237–45
[17] Arkadiev V A, Pogrebkov A K and Polivanov M C 1989 Inverse scattering transform method and soliton solutions for Davey–Stewartson II equation *Physica* D **36** 189–97
[18] Ablowitz M J and Villarroel J 1997 Solutions to the time dependent Schrödinger and the Kadomtsev–Petviashvili equations *Phys. Rev. Lett.* **78** 570–3
[19] Villarroel J and Ablowitz M J 1999 On the discrete spectrum of the nonstationary Shcrödinger equation and multipole lumps of the Kadomtsev–Petviashvili equation *Commun. Math. Phys.* **207** 1–42
[20] Ablowitz M J, Chakravarty S, Trubatch A D and Villarroel J 2000 A novel class of solutions of the non-stationary Schrödinger and the Kadomtsev–Petviashvilli I equation *Phys. Lett.* A **267** 132–46
[21] Pelinovsky D E and Stepanyants Y 1993 New multisoliton solutions of the Kadomtsev–Petvashvili equation *JETP Lett.* **57** 24–28
[22] Dubard P and Matveev V B 2013 Multi-rogue waves solutions: from the NLS to the KP-I equation *Nonlinearity* **26** R93–R125
[23] Chen S, Grelu P, Mihalache D and Baronio F 2016 Families of rational solution solutions of the Kadomtsev Petviashvili I equation *Rom. Rep. Phys.* **68** 1407–24
[24] Chang J-H 2018 Asymptotic analysis of multilump solutions of the Kadomtsev–Petviashvili I equation *Theor. Math. Phys.* **195** 676–89
[25] Hu W, Huang W, Lu Z and Stepanyants Y 2018 Interaction of multi-lumps within the Kadomtsev–Petviasvily equation *Wave Motion* **77** 243–56
[26] Chakravarty S and Zowada M 2022 Dynamics of KPI lumps *J. Phys. A: Math. Theor.* **55** 195701
[27] Yang B and Yang J K 2022 Pattern transformation in higher-order lumps of the Kadomtsev–Petviashvili I equation *J. Nonlinear Sci.* **32** 52
[28] Chakravarty S and Zowada M 2022 Classification of KP I lumps *J. Phys. A: Math. Theor.* **55** 215701
[29] Dong J Y, Ling L M and Zhang X E 2022 Kadomtsev–Petviashvili equation: one-consrranit method and lump pattern *Physica* D **432** 133152
[30] Galkin V M, Pelinovsky D E and Stepanyants Y 1995 The structure of the rational solutions to the Bossinesq eqaution *Physica* D **80** 246–55
[31] Clarkson P A and Dowie E 2017 Rational solutions of the Boussinesq equation and applications to rogue waves *Trans. Math. Appl.* **1** 1–26
[32] Villarroel J, Prada J and Estévez P G 2009 Dynamics of lump solutions in a $2+1$ NLS equation *Stud. Appl. Math.* **122** 395–410
[33] Villarroel J, Prada J and Estévez P G 2017 Weakly decaying solutions of nonlinear Schrödinger equation in the plane *J. Phys. A: Math. Theor.* **50** 495203
[34] Guo L J, He J S and Mihalache D 2021 Rational and semi-rational solutions to the asymmetric Nizhnik–Novikov–Veselov system *J. Phys. A: Math. Theor.* **54** 095703

[35] Ward R S 1995 Nontrivial scattering of localized solitons in a $(2+1)$-dimensional integrable system *Phys. Lett.* A. **208** 203–8
[36] Ioannidou T 1996 Soliton solutions and nontrivial scattering in an integrable chiral model in $(2+1)$ dimensions *J. Math. Phys.* **37** 3422–43
[37] Mañas M and Santini P 1997 Solutions of the Davey–Stewartson II equation with arbitrary rational localization and nontrivial interaction *Phys. Lett.* A. **227** 325–34
[38] Villarroel J and Ablowitz M J 2003 On the discrete spectrum of systems in the plane and the Davey–Stewartson II equation *SIAM J. Math. Anal.* **34** 1253–78
[39] Fokas A S, Pelinovsky D E and Sulem C 2001 Interaction of lumps with a line soliton for the DSII equation *Physica* D **152** 189–98
[40] Kou X 2014 Rogue wave solutions to integrable system by Darboux transformation *Master's Thesis* Department of Mathematics and Statistics, University of Vermont
[41] Guo L J, Wang L H, Cheng Y and He J S 2017 High-order rogue wave solutions of the classical massive Thirring model equations *Commun. Nonlinear Sci. Numer. Simul.* **52** 11–23
[42] Guo L J, Wang L H, Cheng Y and He J S 2019 Higher-order rogue waves and modulation instability of the two-component derivative nonlinear Schrodinger equation *Commun. Nonlinear Sci. Numer. Simul.* **79** 104915
[43] Yang B and Yang J K 2019 Rogue waves in the nonlocal PT-symmetric nonlinear Schrodinger equation *Lett. Math. Phys.* **109** 945–73
[44] Mu G, Qin Z Y, Grimshaw R and Akhmediev N 2019 Intricate dynamics of rogue waves governed by the Sasa–Satsuma equation *Physica* D **402** 132252
[45] Liu C and Akhmediev N 2019 Super-regular breathers in nonlinear systems with self-steepening effect *Phys. Rev.* E **100** 062201
[46] Ling L M, Feng B-F and Zhu Z N 2018 General soliton solutions to a coupled Fokas–Lenells equation *Nonlinear Anal.: Real World Appl.* **40** 185–214
[47] Zhang G Q, Yan Z Y and Wang L 2018 The general coupled Hirota equations: modulational instability and higher-order vector rogue wave and multi-dark solitons tructures *Proc. R. Soc.* A **475** 0625
[48] Wang L H, He J S, Xu H, Wang J and Porsezian K 2017 Generation of higher-order rogue waves from multibreathers by double degeneracy in an optical fiber *Phys. Rev.* E **95** 042217
[49] He J S, Zhang H R, Wang L H, Porsezian K and Fokas A S 2013 Generating mechanism for higher-order rogue waves *Phys. Rev.* E **87** 052914
[50] Guo B, Ling L and Liu Q P 2012 Nonlinear Schrödinger equation: generalized Darboux transformation and rogue wave solutions *Phys. Rev.* E **85** 026607
[51] Baronio F, Conforti M, Degasperis A and Lombardo S 2013 Rogue Waves emerging from the resonant interaction of three waves *Phys. Rev. Lett.* **111** 114101
[52] Mu G, Qin Z Y, Grimshaw R and Akhmediev N 2020 Intricate dynamics of rogue waves governed by the Sasa–Satsuma equation *Physica* D **402** 132252